ENVIRONMENTAL RESEARCH
COMMUNICATIONS

LETTER • OPEN ACCESS

Contribution of anthropogenic and hydroclimatic factors on the variation of surface water extent across the contiguous United States

To cite this article: Irene Palazzoli *et al* 2023 *Environ. Res. Commun.* **5** 051006

Environmental Research Communications

CrossMark

OPEN ACCESS

RECEIVED
20 January 2023

REVISED
17 March 2023

ACCEPTED FOR PUBLICATION
12 May 2023

PUBLISHED
22 May 2023

LETTER

Contribution of anthropogenic and hydroclimatic factors on the variation of surface water extent across the contiguous United States

Irene Palazzoli , **Alberto Montanari** and **Serena Ceola**

Department of Civil, Chemical, Environmental and Materials Engineering, Alma Mater Studiorum, Università di Bologna, Bologna, 40136, Italy

E-mail: irene.palazzoli@unibo.it

Keywords: surface water resources, human pressure, irrigation, urbanization, hydroclimatic variability, climate classification

Supplementary material for this article is available online

Abstract

Human pressure and climate variability are significantly threatening freshwater resources, with cascading effects on societies and ecosystems. In this context, it is crucial to understand the anthropogenic and climatic impacts on surface water dynamics. Here, we examine the interaction between the variation of surface water extent and the change in five potential concurrent drivers across river basins of the contiguous United States (CONUS) during the period 1984–2020. In particular, built-up area, population, and irrigated land are regarded as the anthropogenic drivers, while hydroclimatic drivers are represented by precipitation and potential evapotranspiration (PET). We perform statistical analyses in order to quantify the change in the considered variables and then identify significantly different spatial patterns and possible interrelations. Results show that almost 79% (169 out of 204 river basins) of the CONUS experienced an expansion of surface water extent mainly in the continental and temperate climatic regions (mean expansion 158.33 km^2). Increasing precipitation is found to be the most widespread driver of the gain in surface water extent, affecting nearly 70% of river basins. The remaining 35 river basins of the CONUS, mostly located in the arid southwestern region of the country, faced a reduction in surface water extent (mean reduction −146.73 km^2). The expansion of built-up areas and increasing PET resulted to contribute to the loss of surface water in all the river basins, followed by population growth (in ~75% of the river basins), decreasing precipitation (in ~60% of the river basins, all situated in southwestern US), and irrigated land expansion (in ~55% of the river basins). Our findings shed light on the potential impacts of the variability of anthropogenic and hydroclimatic factors on hydrology and surface water resources, which could support predictive adaptation strategies that ensure water conservation.

1. Introduction

Water is a major and unique resource for humans and the environment. Among all water resources, surface waters, i.e., any water body that is above the ground, such as streams, rivers, lakes, and wetlands, are vital sources for preserving the biodiversity of aquatic and terrestrial ecosystems (Poff *et al* 1997, Dooge 2009, Vörösmarty *et al* 2010). They also constitute an indispensable element for the economic wealth of society, by suppling water for drinking, agricultural, and industrial purposes from local to global scale (FAO 2017, Wang and Xie 2018, Wang *et al* 2020). However, natural and human-induced factors reshape surface water bodies, by shrinking and expanding their extent, or moving their location with time (Granzotti *et al* 2018, Palazzoli *et al* 2022). As a result, surface water extent and availability are changing at the global scale and future population growth and climate change stress the need to keep these dynamics under sustainable levels (Kummu *et al* 2016, Rodell *et al* 2018, FAO 2020).

Climate variability significantly affects the whole hydrologic cycle by causing spatiotemporal variations of precipitation, temperature, evapotranspiration, and soil moisture, which modify the amount, distribution pattern, and timing of available surface water (Zhuang *et al* 2018, Duan *et al* 2019, IPCC *et al* 2021). In particular, extreme events determined by precipitation and temperature variability, e.g., droughts and floods, seriously impact surface waters (Brunner *et al* 2021, McKinnon and Deser 2021).

Through history humans have learnt how to control and exploit water resources exerting a critical and constantly increasing pressure on the hydrological cycle (Ceola *et al* 2015, Wada *et al* 2017). Growing population, urbanization, and economic development are expected to produce 55% increase of water demand in the manufacturing, thermal electricity generation, and domestic uses by 2050 (Paterson *et al* 2015, Grizzetti *et al* 2017, Ceola *et al* 2019). Similarly, the irrigated food production will increase by more than 50% by 2050 (Mancosu *et al* 2015, Nie *et al* 2021), causing extensive water abstractions, especially in arid and semi-arid regions, which are likely to experience water scarcity (Starr & Levison 2014, FAO 2020). Furthermore, dams and reservoir significantly alter surface water extent as well as the flow regime and morphology of rivers (Lin 2011, Da Silva *et al* 2020, Di Baldassarre *et al* 2021). Therefore, it is fundamental to understand how changes in anthropogenic and hydroclimatic factors induce variations in surface water extent (Palazzoli 2022).

We hereby examine how surface water extent and potential anthropogenic and hydroclimatic drivers have changed from 1984 to 2020 across river basins of the contiguous United States (CONUS). Long-term, spatially-explicit, and high-resolution remote sensing data are employed to address the following crucial questions: (i) how much have surface water extent, anthropogenic pressure, and climate changed in the last 40 years across the CONUS? (ii) are there any specific spatial patterns in these changes? (iii) what is the influence of changes in anthropogenic and hydroclimatic drivers on changes in surface water extent? To this aim, we identify built-up area, population, and irrigation dynamics as relevant anthropogenic drivers, while precipitation and potential evapotranspiration (PET) are here considered as key hydroclimatic drivers. Afterwards, we split our study period into two epochs, 1984–1999 and 2000–2020, to analyze the variation of surface water extent and its drivers at the river basin level across the CONUS.

2. Methods

2.1. The contiguous united states

Our investigation focuses on the study area of the contiguous United States (CONUS) as it embeds heterogeneous hydroclimatic and socio-economic conditions, offering the opportunity to explore a large and composite territory, encompassing both wet and dry regions, with a spatially-varying topography, surface water availability (Dettinger *et al* 2015, Tidwell *et al* 2017), and degree of urbanization (Sun and Caldwell 2015, Fang and Jawitz 2019). 204 river basins, corresponding to the 4-digit hydrologic units (HUC-4s) delineated following the definition provided by the USGS (Seaber *et al* 1987), are employed in this study (figure 1(a)). The Köppen-Geiger climate classification system (Beck *et al* 2018) is used to describe the climatic conditions of the CONUS (Figure S1).

2.2. Data

2.2.1. Surface water extent

The Surface Water Occurrence Change Intensity layer from the Global Surface Water dataset (Pekel *et al* 2016) is employed to define the change in surface water extent (SWE). This product shows where surface water occurrence increased, decreased or remained invariant between two epochs (1984–1999 and 2000–2020) describing both the direction of change and its intensity in terms of percentage at a 30 m spatial resolution. Here, a 75% intensity of change is selected as a representative value identifying locations that experienced a significant and permanent change in SWE, insensitive to seasonal variations. Pixels of the Water Occurrence Change Intensity layer having a value between −100% and −75% detect locations that encountered a surface water loss between the two epochs, while those having a value between 75% and 100% indicate locations of surface water gain. In this way, we create the Surface Water Loss and Surface Water Gain binary maps (figure 1(b)).

2.2.2. Anthropogenic drivers

The Global Human Settlement Layer dataset (Corbane *et al* 2019) is used as input data to estimate the extent of built-up areas (BUP) and the distribution of population (POP). The GHS-BUILT layer provides a multi-temporal classification of BUP, showing the location of built-up areas developed before 1975, between 1975 and 1990, between 1990 and 2000, and between 2000 and 2014 at a spatial resolution of 30 m. The GHS-BUILT layer is here considered to provide a reliable representation of the impact of urban areas, human settlements, and human activities on surface water resources (e.g., domestic and industrial uses, development of impervious areas leading to river fragmentation). According to the definition of the two epochs here considered, for this analysis

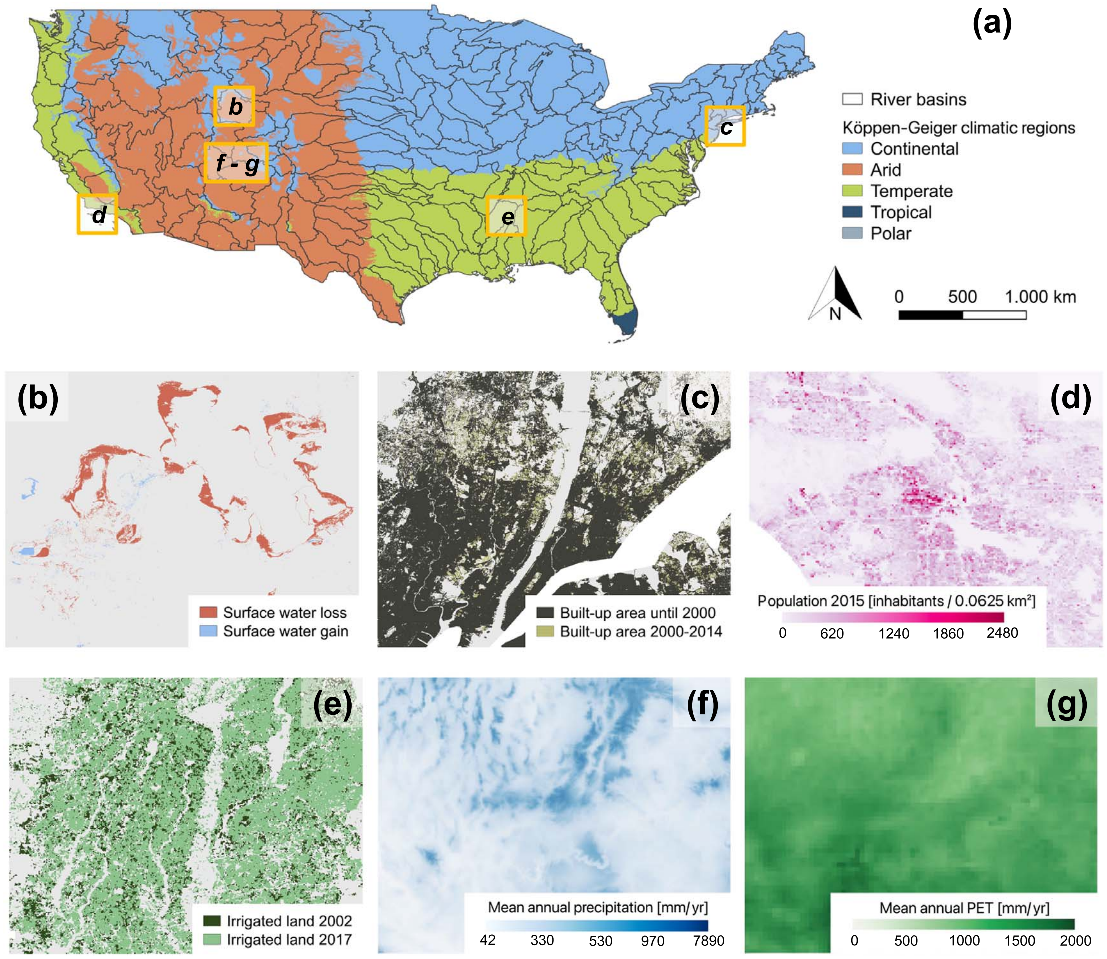

Figure 1. Change in surface water extent and anthropogenic and hydroclimatic factors across the CONUS from 1984 to 2020. (a) River basins and climate classification, according to USGS HUC-4s and Köppen-Geiger system, respectively, and location of the zoom-in areas shown in panels b-g. (b) Surface Water Gain and Surface Water Loss over the region around the Great Salt Lake, derived from the Global Surface Water dataset (Pekel *et al* 2016). (c) Built-up area developed before and after 2000 over the region around New York City, derived from the Global Human Settlement Layer dataset (Corbane *et al* 2019). (d) Population distribution in 2015 over the region around the city of Los Angeles, derived from the Global Human Settlement Layer dataset (Corbane *et al* 2019). (e) Irrigated land in 2002 and 2017 over the region between Little Rock and Memphis, derived from the Irrigated Agriculture Dataset for the United States, MODIS-MirAD-US (Pervez & Brown 2010). (f) Mean annual precipitation in the period 2000–2020 over the region around the Grand Canyon and the Colorado River, derived from Daymet Version 4 dataset (Thornton *et al* 2020). (g) Mean annual PET in the period 2000–2020 over the region around the Grand Canyon and the Colorado River, derived from the hourly PET (hPET) dataset (Singer *et al* 2021).

we identified built-up locations developed before 1975, between 1975 and 1990, and between 1990 and 2000 as representative of the urban development before the year 2000, while the most recent built-up extent (i.e., after the year 2000) includes all the built-up locations described in the GHS-BUILT layer (figure 1(c)). Similarly, the GHS-POP layer describes the distribution of population observed in four years (1975, 1990, 2000, and 2015) as the number of people per cell with a spatial resolution of 250 m. From the GHS-POP layer it is possible to infer the influence that inhabitants only produce on surface waters. For this analysis, the number of inhabitants observed until 2000 and until 2015 define the distribution of population before and after the year 2000, respectively (figure 1(d)).

Data of irrigated land (IRR) are complementary to built-up areas and population distribution, as they provide an estimate of the anthropogenic surface water use for irrigation purposes. The extent of irrigated land was obtained from the Irrigated Agriculture Dataset for the United States (MODIS MirAD-US), which supplies irrigation data for four years (2002, 2007, 2012, and 2017) at 250 m spatial resolution (Pervez & Brown 2010). In particular, we select the areas of irrigated agriculture observed in 2002 and 2017 as representative of the periods before and after the year 2000, respectively (figure 1(e)).

2.2.3. Hydroclimatic drivers

The hydroclimatic variability over the period of 37 years is here estimated as changes in precipitation and PET. The Daymet Version 4 dataset, developed with ground-based meteorological observations, provides total annual precipitation (in mm/yr) at a spatial resolution of 1 km (Thornton *et al* 2020). We derive mean annual precipitation values (MAP) representative of the 1984–1999 and 2000–2020 epochs by averaging the total annual precipitation (figure 1(f)). Regarding temperature, data and methodology adopted for the assessment of temperature change are described in the Supporting Material.

2.3. Analysis of changes in surface water extent and its drivers

In order to evaluate the contribution of the change in anthropogenic (BUP, POP, and IRR) and hydroclimatic (MAP and PET) drivers on the change in SWE before and after the year 2000, we aggregate the local-scale high resolution data previously described at the river basin (HUC-4s) level (Palazzoli 2022). The difference in the spatial resolution do not affect the aggregation at the river basin level, since river basins are fully resolved in our data.

Given a generic river basin b, we assume that the net change in SWE occurred in this basin, ΔSWE_b, can be expressed as a combination of changes in the anthropogenic and hydroclimatic drivers as follows:

$$\Delta SWE_b = f(\Delta BUP_b, \Delta POP_b, \Delta IRR_b, \Delta MAP_b, \Delta PET_b) \tag{1}$$

More specifically, the net change in surface water extent at the river basin level ΔSWE_b (km^2) is calculated from the binary maps of Surface Water Gain and Surface Water Loss, considering both the direction and the over-threshold intensity of change, as:

$$\Delta SWE_b = \sum_{i=1}^{n_b} g(i) - \sum_{i=1}^{n_b} l(i) \tag{2}$$

where *i* is a generic pixel in the considered river basin b, n_b is the total number of pixels in *b*, *g*(*i*) (or *l*(*i*)) is equal to the pixel area ($9\cdot10^{-4}$ km^2) if *i* experienced a gain (or loss) in the study period, otherwise it is null.

The change in built-up area at the river basin level, ΔBUP_b (km^2), before and after year 2000, reads as follows:

$$\Delta BUP_b = \sum_{i=1}^{n_b} BUP_{2000-2020}(i) - \sum_{i=1}^{n_b} BUP_{1984-1999}(i) \tag{3}$$

where $BUP_{1984-1999}(i)$ (or $BUP_{2000-2020}(i)$) corresponds to the pixel area ($9\cdot10^{-4}$ km^2) if i is classified as a built-up location during 1984–1999 (or 2000–2020), otherwise it is null.

The change in population at the river basin level, ΔPOP_b (number of inhabitants), before and after year 2000, is:

$$\Delta POP_b = \sum_{i=1}^{n_b} POP_{2000-2020}(i) - \sum_{i=1}^{n_b} POP_{1984-1999}(i) \tag{4}$$

where $POP_{1984-1999}(i)$ (or $POP_{2000-2020}(i)$) corresponds to total population (number of inhabitants) observed in i during 1984–1999 (or 2000–2020).

The change in irrigated land area at the river basin level, ΔIRR_b (km^2), before and after year 2000, reads as follows:

$$\Delta IRR_b = \sum_{i=1}^{n_b} IRR_{2000-2020}(i) - \sum_{i=1}^{n_b} IRR_{1984-1999}(i) \tag{5}$$

where $IRR_{1984-1999}(i)$ (or $IRR_{2000-2020}(i)$) corresponds to the pixel area ($6.25\cdot10^{-2}$ km^2) if i is classified as an irrigated land location during 1984–1999 (or 2000–2020), otherwise it is null.

The change in mean annual precipitation at the river basin level, ΔMAP_b (mm/yr), before and after the year 2000, is estimated by computing the difference between the spatial average of local values as follows:

$$\Delta MAP_b = \frac{\sum_{i=1}^{n_b} MAP_{2000-2020}(i)}{n_b} - \frac{\sum_{i=1}^{n_b} MAP_{1984-1999}(i)}{n_b} \tag{6}$$

where $MAP_{1984-1999}(i)$ (or $MAP_{2000-2020}(i)$) is the mean annual precipitation measured in pixel i during 1984–1999 (or 2000–2020).

Finally, the change in PET at the river basin level, ΔPET_b (mm/yr), before and after the year 2000, is defined as the difference between the spatial average of pixel-based mean annual PET, which reads:

$$\Delta PET_b = \frac{\sum_{i=1}^{n_b} PET_{2000-2020}(i)}{n_b} - \frac{\sum_{i=1}^{n_b} PET_{1984-1999}(i)}{n_b} \tag{7}$$

where $PET_{1984-1999}(i)$ (or $PET_{2000-2020}(i)$) is the mean annual PET measured in pixel i during 1984–1999 (or 2000–2020).

Afterwards, we check for significantly distinct spatial patterns of ΔSWE_b, ΔBUP_b, ΔPOP_b, ΔIRR_b, ΔMAP_b, and ΔPET_b based on the prevalent climatic characteristics of each river basin, according to the Köppen-Geiger classification, by applying the Kruskal-Wallis test (see Supporting Material for more details).

To test the hypothesis that surface water extent varies as a consequence of the variation in the anthropogenic and hydroclimatic drivers, first we check for any correlation among the considered variables. Then, we divide river basins experiencing $\Delta SWE_b > 0$ from those facing $\Delta SWE_b < 0$ and we compare ΔSWE_b against the direction of change of each driver in order to determine their relevance (i.e., we assume that $\Delta BUP_b < 0$, $\Delta POP_b < 0$, $\Delta IRR_b < 0$, $\Delta MAP_b > 0$, and $\Delta PET_b < 0$ should contribute to $\Delta SWE_b > 0$, whereas $\Delta BUP_b > 0$, $\Delta POP_b > 0$, $\Delta IRR_b > 0$, $\Delta MAP_b < 0$, and $\Delta PET_b > 0$ should contribute to $\Delta SWE_b < 0$). Afterwards, we evaluate the Pearson's correlation coefficient, r, between the positive and negative variations of SWE and each driver, by also considering groups of river basins sharing the same prevailing climatic condition. Finally, a Principal Components Analysis (PCA) is carried out to reduce the dimensionality of the considered dataset.

3. Results

3.1. Spatial and climatic patterns of basin-scale change in surface water extent and anthropogenic and hydroclimatic drivers

The majority of the CONUS (169 river basins covering 78.64% of the study area) experienced a net gain of surface water extent ($\Delta SWE_b > 0$), while a net loss of surface water ($\Delta SWE_b < 0$) is found in the remaining 35 river basins (figure 2(a)). By grouping river basins according to their prevalent Köppen-Geiger climatic region, we find that river basins with a continental and temperate climate experienced on average a net increase of surface water extent, while those having an arid climate present on average a mild decrease of surface water (figures 2(b) and S2). Since the tropical climate is prevalent only in a single river basin located in Southern Florida, no statistically-robust prediction can be inferred for river basins with these climatic conditions. The distinct behavior of ΔSWE_b as a function of the main climatic region is also confirmed by the Kruskal-Wallis test, showing statistically significant differences among river basins with arid and continental climates, arid and temperate climates, continental and temperate climates (Table S1).

When analyzing changes in anthropogenic drivers, we find $\Delta BUP_b > 0$ for all river basins, since built-up area extent increased from 1984–1999 to 2000–2020, especially over the Eastern US and along the West Coast (figure 2(c)). The largest built-up area expansion results to have occurred in river basins with a temperate climate, followed by those with a continental and arid climate (figure 2(d)). The Kruskal-Wallis test shows that ΔBUP_b presents distinct trends as a function of the main climatic regions, with statistically significant differences between river basins with arid and continental and arid and temperate climates (Table S1).

With reference to population, we observe $\Delta POP_b > 0$ in most of the river basins (167, covering 81.55% of the CONUS), while a decreasing trend in population ($\Delta POP_b < 0$) is found across the remaining 37 river basins, mainly located in the northeastern and the central area of the country (figure 2(e)). In particular, population increased the most in river basins with a dominant temperate climate, followed by arid and continental climates (figure 2(f)). Also in this case, statistically significant differences are found in terms of ΔPOP_b as controlled by the climatic classification. Moreover, the climatic groups that markedly differ from each other are arid and temperate and continental and temperate climates (Table S1).

Regarding the extent of irrigated land, we find $\Delta IRR_b > 0$ in 136 river basins (67.47% of the CONUS), while in the remaining 68 river basins irrigated agriculture shrank, especially in the western region of the CONUS (figure 2(g)). ΔIRR_b increased the most in river basins with a continental and temperate climate, while in river basins with an arid climate the change in the extent of irrigated land was less pronounced (figure 2(h)). The difference between ΔIRR_b values grouped as a function of climatic regions results to be statistically significant, with only arid and continental climates presenting remarkable differences (Table S1).

With reference to the changes in hydroclimatic variables, we find $\Delta MAP_b > 0$ in 132 river basins (54.64% of the CONUS), the majority of which is located in Eastern US, while the remaining 72 river basins, characterized by $\Delta MAP_b < 0$, are found in Western US (figure 2(i)). More specifically, as shown in figure 2(j), ΔMAP_b increased the most in continental and temperate climates, while it generally decreased in arid climates. Statistically significant differences of ΔMAP_b emerge according to climatic regions, especially between arid and continental and arid and temperate climates (Table S1).

Concerning PET change, most of the river basins of the CONUS (198 out of the 204, covering 96.52% of the CONUS) experienced $\Delta PET_b > 0$ (figure 2(k)). In particular, ΔPET_b increased the most in arid climates, followed by temperate and continental climates (figure 2(l)). Also in this case, remarkable differences in ΔPET_b are found, in particular between arid and continental climates, arid and temperate climates, and continental and temperate climates (Table S1).

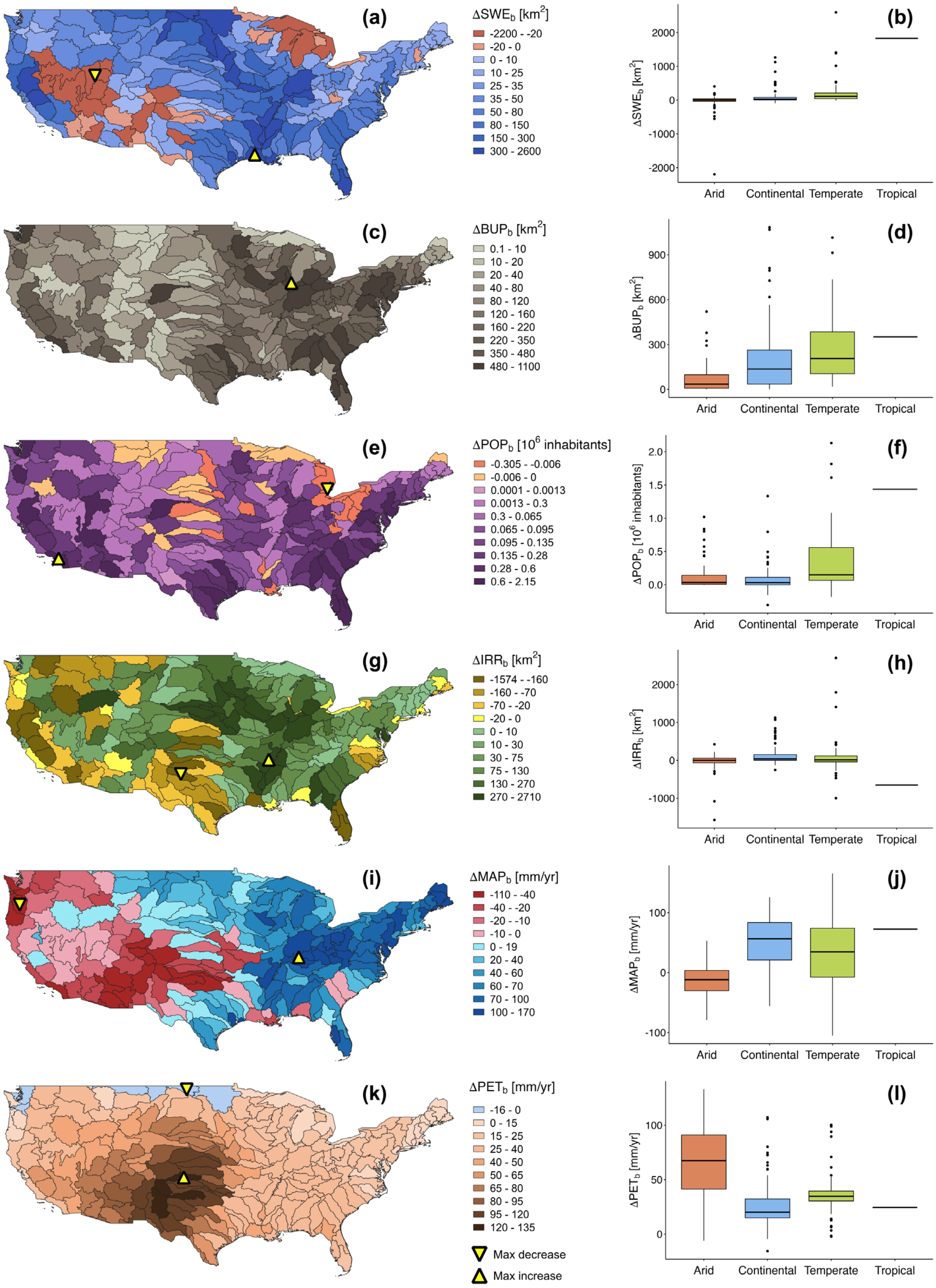

Figure 2. Spatial and climatic patterns of basin-scale change in surface water extent, anthropogenic and hydroclimatic drivers occurred between 1984–1999 and 2000–2020 across the CONUS. The left column shows the spatial distribution, where river basins experiencing the maximum increase and decrease are highlighted with an upward and downward yellow triangle, respectively (for more details, see Supporting Material). The right column shows boxplots of changes grouped according to the prevalent Köppen-Geiger climatic region of each river basin. The boxplot edges indicate the first and third quartiles, with the thick horizontal line representing the median value. (a), (b) Net change in surface water extent, ΔSWE_b. (c), (d) Change in built-up area extent, ΔBUP_b. (e), (f) Change in total population, ΔPOP_b. (g), (h) Change in irrigated land, ΔIRR_b. (i), (j) Change in mean annual precipitation, ΔMAP_b. (k), (l) Change in mean annual PET, ΔPET_b.

Overall, the largest variations in SWE, BUP, POP, IRR, and MAP within the temperate and continental regions (boxplots in figure 2), while the largest change in PET and TMP is observed in arid areas (figures 2(l) and S4(b)). A comparable distribution of changes is found at the climatic subtype level (Figures S3 and S5), with the

Table 1. Correlation (Pearson's r coefficient) between the change in surface water extent and its anthropogenic and hydroclimatic drivers. River basins are grouped according to the direction of change in surface water extent and to the main climatic conditions. Only one river basin of the CONUS has a tropical climate, thus no correlation is found within this climatic group. Cross correlation values among drivers are reported in table S2.

		All river basins	Arid	Continental	Temperate
$\Delta SWE_b>0$	# of basins	169	34	74	60
	ΔBUP_b	0.051	0.067	0.007	−0.072
	ΔPOP_b	0.104	−0.019	0.004	−0.113
	ΔIRR_b	0.202	−0.119	0.297	0.315
	ΔMAP_b	0.080	0.486	−0.135	0.114
	ΔPET_b	−0.074	−0.577	0.018	0.033
$\Delta SWE_b<0$	# of basins	35	24	10	1
	ΔBUP_b	0.165	0.319	0.101	—
	ΔPOP_b	0.433	0.402	−0.270	—
	ΔIRR_b	−0.078	−0.033	0.141	—
	ΔMAP_b	−0.075	0.211	0.188	—
	ΔPET_b	−0.087	−0.368	−0.331	—

continental region with no dry season and cold summer having the most remarkable increasing trends in SWE, BUP, and POP and the largest reduction in IRR. Whereas, all the arid subtypes show the largest decrease in SWE corresponding to the largest increase in PET and TMP. Additional results based on temperature anomalies (ΔTMP_b) are provided in figures S4, S5, and table S1 of the Supporting Material.

3.2. Contribution of anthropogenic and hydroclimatic drivers on changes in surface water extent

In order to verify if the variations in the considered anthropogenic and hydroclimatic drivers observed before and after the year 2000 may have influenced the expansion and shrinkage of surface waters that occurred during the same time period, we first explore any correlation among variables and we then assess the overlap between the directions of change, by distinguishing between river basins experiencing either a net gain ($\Delta SWE_b > 0$) or a net loss ($\Delta SWE_b < 0$) in surface water extent.

Concerning the interdependency among drivers, we find mild to low correlations (Table S2), except for ΔBUP_b and ΔPOP_b ($r = 0.71$ for all river basins, reaching its maximum value equal to 0.92 in arid river basins experiencing $\Delta SWE_b > 0$). Based on these results and given that, in most of the climatic regions, the datasets employed for estimating ΔBUP_b and ΔPOP_b provide similar, though complementary information, all anthropogenic and hydroclimatic drivers are considered in the forthcoming analysis.

Then we look at the correlation between ΔSWEb and all the drivers, either distinguishing or not for the gain or loss of SWE (*table* 1) and for the main climatic classification (Table S2). Generally, we find low to mild correlations, with larger values ($|r| > 0.4$) only across arid areas and between the gain in SWE and changes in population. Similar results also emerge from the PCA, where we divided river basins with $\Delta SWE_b>0$ from $\Delta SWE_b<0$. Focusing on the river basins with $\Delta SWE_b>0$, we find a clear distinction along PC1 (explaining 38.76% of the total variance, see also figure S6(a) for PCA eigenvalues) between river basins with an arid climate, primarily associated to negative values of PC1, and river basins with a temperate and continental climate, distributed over both positive and negative values of PC1 (figure 3(a)). The magnitude and direction of the coefficients associated to the original variables (vectors in figure 3(a)) reveal that changes in built-up area, population, and precipitation are the drivers that affect the most PC1. On the other hand, PC2 is mostly influenced by the climatic drivers (positive and negative association with precipitation and PET, respectively) and irrigated land (positive association). Moving to the group of river basins with $\Delta SWE_b<0$, the PCA shows a remarkable and clear distinction between clusters of river basins with different climatic conditions (figure 3(b)), with the 24 arid river basins mainly located along the negative values of PC1 (explaining the 40.34% of the total variation, see also figure S6(b)), while the remaining 11 river basins (10 with a continental climate and one with a temperate climate) are associated to positive values of PC1. Precipitation and PET are the variables contributing the most to the first component PC1, whereas the anthropogenic factors are those influencing the most PC2.

Regarding the overlap among direction of change of the drivers, we find that the most widespread driver concurring to $\Delta SWE_b > 0$ is $\Delta MAP_b > 0$, observed in the majority of river basins (118 out of 169, covering 50.22% of the CONUS), mainly located in the eastern region of the CONUS (figure 4(a)). All the remaining drivers contribute to $\Delta SWE_b > 0$ in less than 30% of the river basins, with $\Delta BUP_b < 0$ never contributing (figure 4(b)). A simultaneous contribution of all drivers, except for built-up areas, to $\Delta SWE_b > 0$ is observed in 2 river basins only (1.48% of the CONUS), while none of the drivers concur to an increase in surface water extent across 23 river basins (11.51% of the CONUS).

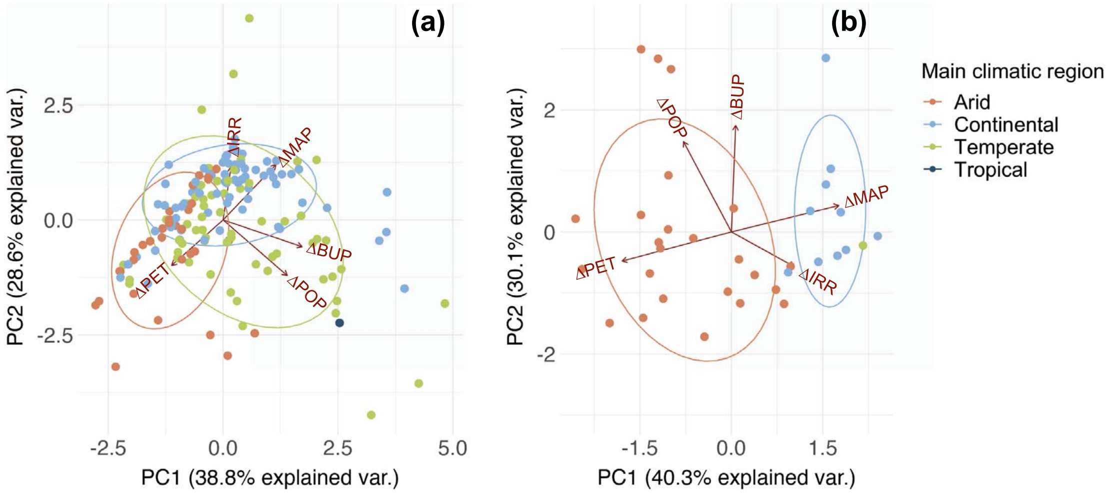

Figure 3. Biplots for changes in anthropogenic (ΔBUP_b, ΔPOP_b, and ΔIRR_b) and hydroclimatic (ΔMAP_b and ΔPET_b) drivers (correlation matrix PCA). (a) River basins with $\Delta SWE_b > 0$. (b) River basins with $\Delta SWE_b < 0$. Data are colored based on the prevalent climatic condition associated to each river basin. Labeled vectors (arrows) indicate the loadings, i.e., the magnitude and direction of influence of each driver along the principal components. The ellipses represent the core area with a confidence interval of 68%, highlighting the separation between the observation groups.

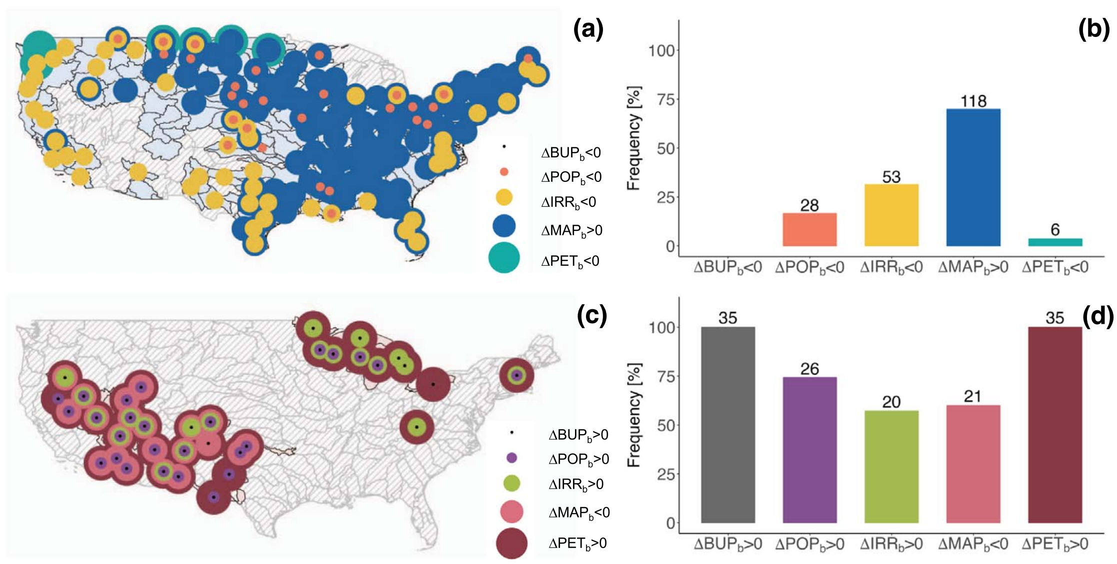

Figure 4. Spatial overlap of potential contributors to a change in surface water extent. (a) River basins with $\Delta SWE_b > 0$, supposed to be triggered by $\Delta BUP_b < 0$ (black circle), $\Delta POP_b < 0$ (orange circle), $\Delta IRR_b < 0$ (yellow circle), $\Delta MAP_b > 0$ (blue circle), and $\Delta PET_b < 0$ (cyan circle). (b) Frequency of occurrence of each anthropogenic and hydroclimatic driver to $\Delta SWE_b > 0$, where values over the bin of each contributor indicate the number of river basins. (c) River basins with $\Delta SWEb < 0$, supposed to be triggered by $\Delta BUPb > 0$ (black circle), $\Delta POPb > 0$ (purple circle), $\Delta IRRb > 0$ (green circle), $\Delta MAPb < 0$ (pink circle), and $\Delta PETb > 0$ (red circle). (d) Frequency of occurrence of each anthropogenic and hydroclimatic driver to $\Delta SWEb < 0$, where values over the bin of each contributor indicate the number of river basins.

Within the group of river basins with $\Delta SWE_b < 0$, we find that all anthropogenic and hydroclimatic drivers significantly contributed to this condition, with more than 50% of river basins for each driver and with both ΔBUP_b and ΔPET_b increasing in all the 35 river basins (figures 4(c), (d)). A simultaneous contribution of all drivers to a net loss in SWE is found in 8 river basins (10.65% of the CONUS).

4. Discussion and conclusions

In order to prevent uncontrolled alterations of hydrological cycle and support predictive adaptation strategies in response to the impacts of human dynamics and climate variability on water resources, it is fundamental to investigate the extent to which anthropogenic and hydroclimatic factors influence variations of surface water bodies. Benefiting from the use of long-term, spatially-explicit, and high-resolution remote sensing data, we explore how SWE and potential anthropogenic and hydroclimatic drivers have changed from 1984 to 2020 across the river basins of the CONUS.

Some limitations need to be acknowledged. Our study focuses on surface water resources, neglecting the groundwater component, even though it often constitutes a critical source of water, especially for irrigation purposes in arid areas of the US. We restrict the analysis to surface waters as in 2015 they represented the main source of water in the US, accounting for 74% water withdrawals of the country, with many western states used surface water as their primary source also for irrigation (Dieter *et al* 2018). From a methodological point of view, global estimates of the anomalies in the Terrestrial Water Storage (TWS) provided by the Gravity Recovery and Climate Experiment (GRACE) dataset (Rodell *et al* 2018) may be employed to derive data of groundwater dynamics. However, GRACE spatial resolution (~50 km at the equator) is much coarser compared to that of the Global Surface Water dataset (30 m). In addition, GRACE temporal coverage does not go back further than 2002. Yet, future analysis should include groundwater to account for impacts caused by irrigation and climate variability on water storage of river basins.

Another constraint comes from the use of the Global Surface Water dataset to estimate changes in surface water extent. In particular, the adoption of data from the Surface Water Occurrence Change Intensity layer (Pekel *et al* 2016) led us to evaluate changes in both anthropogenic and hydroclimatic factors within the epochs 1984–1999 and 2000–2020, to estimate variations over the same temporal windows. This approach does not allow to examine changes that might occur at a finer temporal resolution, rather than within a 20-year period. However, the choice of the Global Surface Water dataset, instead of other existing surface water datasets, relies on the advantage that it meets our need for data describing long-term changes in surface water bodies at high spatial resolution (Yamazaki *et al* 2015).

An additional limitation is associated to irrigation data. The MIrAD-US dataset, here employed to determine changes in the extent of irrigated agriculture, was developed using a combination of remotely sensed data and irrigation statistics and census. We acknowledge that satellite images allow to monitor high spatial and temporal variability of irrigated land, yet they might be unable to detect the presence of irrigated areas in humid regions that overall may produce a remarkable amount of water consumption (Pervez and Brown 2010). Furthermore, irrigation statistics and census may produce a lack of accuracy due to surveyed data that rely on surveys and questionnaires as well as self-reported information (Thenkabail *et al* 2009, Ajaz *et al* 2019). However, the overall mapping of irrigated land here employed is still superior to other existing products of irrigated agriculture in the CONUS (Pervez and Brown 2010).

Besides these shortcomings, our analysis is able to unravel the interrelations between dynamics of surface water extent, human pressure, and climate variability at the regional level (river basin scale).

Our results show that the majority of the CONUS experienced a net gain of SWE, with only 35 river basins out of the 204 of the study area facing a reduction of their water surfaces. The increase in the extent of surface water involved areas mainly characterized by temperate and continental climatic conditions, while the decrease in surface water was for the most part observed within the arid southwestern region of the US and in some measure within river basins located in the Northeast with a temperate climate.

Variations in the headwaters of a large basin might control changes on its downstream river basins. To account for this, we assess changes in SWE and its drivers across the 18 water resource regions (WRRs) of the CONUS (Figure S7 and figure S8), corresponding to the 2-digit hydrologic units, HUC-2s, defined in Seaber *et al* (1987). Changes in the extent of surface water at the WRR scale (ΔSWE_{WRR}) overall reproduce those observed at the river basin level, with most of the WRRs (14 WRRs) experiencing an expansion of SWE and only 4 WRRs in the arid southwestern US facing a reduction of surface water (Figure S7), yet some interesting findings emerge. In particular, despite a $\Delta SWE_{WRR} > 0$ is found for the Rio Grande Region (WRR 13) and the Lower Colorado Region (WRR 15), their downstream river basins face a net loss of SWE. Conversely, the Arkansas-White-Red Region (WRR 11) shows a gain in SWE, yet its downstream river basin exhibits a decreasing trend.

These results on variations in SWE at the WRR level well compare with recent findings on changing river discharge (Shi *et al* 2019). Indeed, trends in annual river discharge for the period 1960–2010 perfectly agree with the expansion in SWE that we observe across the Mississippi and Colorado Rivers (WRRs 8, 10, 11, and WRRs 14, 15, respectively) and the reduction in SWE across the St. Lawrence, Rio Grande, and Columbia Rivers (WRRs 4, 13, and 17, respectively).

In our analysis, increasing precipitation results to be the major driver of a net gain in SWE (around 75% of 169 river basins, mainly located over the eastern area of the CONUS), while urbanization and temperature rise are found to be the most widespread factors influencing a net loss in SWE (100% of 35 river basins), thus confirming recent findings by Scanlon *et al* (2021). Therein, the role of climatic and human drivers on the variability of the Terrestrial Water Storage (TWS) observed in 14 major US aquifers during the period 2002–2017 was investigated. Although TWS includes groundwater component as well, similarities between the observed changes in TWS and SWE further validate our study. The TWS increase in the eastern and northwestern region of the US favoured by low drought intensity is in agreement with the gain in SWE and the associated increasing precipitation that we observed in our data. Moreover, the substantial reduction of TWS in southwestern US that emerged in Scanlon *et al* (2021) matches the loss of SWE that we find in the same area (see figure 2(a), where the yellow downward triangle identifies the river basin with the largest decrease in SWE). Across this region, Scanlon *et al.* also found the highest correlation between precipitation variability and TWS anomalies, which is consistent with our findings (see correlation between ΔSWE_b and ΔMAP_b for river basins with $\Delta SWE_b > 0$ in table 1).

Furthermore, it is likewise relevant to elaborate more on the potential role of reservoirs and dams as an additional anthropogenic driver of changes in SWE. To examine this aspect, we analyze data from the US National Inventory of Dams (including more than 91,000 dams across the CONUS) and find that dams significantly influence the expansion of surface water extent, rather than the reduction, since larger increases in the extent of surface water occur in river basins with a higher number of dams, especially in regions with a continental climate ($r = 0.51$, see figure S9).

Findings from this study clearly highlight how arid areas, besides being exposed to climate variability, are vulnerable to changes in anthropogenic activities as well. By altering surface water extent, anthropogenic and climatic factors might compromise surface water availability, with cascading negative consequences for humans and the environment. In particular, future anthropogenic and climatic dynamics will increase the risk that current human water needs will no longer be satisfied and will pose an increasing stress on ecosystems. Therefore, this study will help sustainable water development and the identification of predictive adaptation strategies that prevent future water shortages induced by climate and human behavior.

Acknowledgement

This study was carried out within the RETURN Extended Partnership and received funding from the European Union Next-GenerationEU (National Recovery and Resilience Plan – NRRP, Mission 4, Component 2, Investment 1.3 – D.D. 1243 2/8/2022, PE0000005).

Data availability statement

No new data were created or analysed in this study.

ORCID iDs

Irene Palazzoli https://orcid.org/0000-0001-8273-2472
Serena Ceola https://orcid.org/0000-0003-1757-509X

References

Ajaz A, Karimi P, Cai X, De Fraiture C and Akhter M S 2019 Statistical data collection methodologies of irrigated areas and their limitations: a review *Irrigation and Drainage* **68** 702–13

Di Baldassarre G, Mazzoleni M and Rusca M 2021 The legacy of large dams in the United States *Ambio* **50** 1798–808

Beck H E, Zimmermann N E, McVicar T R, Vergopolan N, Berg A and Wood E F 2018 Present and future Köppen-Geiger climate classification maps at 1-km resolution *Scientific Data* **5** 180214

Brunner M I, Swain D L, Gilleland E and Wood A W 2021 Increasing importance of temperature as a contributor to the spatial extent of streamflow drought *Environ. Res. Lett.* **16** 024038

Ceola S, Laio F and Montanari A 2015 Human-impacted waters: New perspectives from global high-resolution monitoring *Water Resour. Res.* **51** 7064–79

Ceola S, Laio F and Montanari A 2019 Global-scale human pressure evolution imprints on sustainability of river systems *Hydrol. Earth Syst. Sci.* **23** 3933–44

Corbane C, Pesaresi M, Kemper T, Politis P, Florczyk A J, Syrris V, Melchiorri M, Sabo F and Soille P 2019 Automated global delineation of human settlements from 40 years of Landsat satellite data archives *Big. Earth Data* **3** 140–69

Dettinger M, Udall B and Georgakakos A 2015 Western water and climate change *Ecological Applications* **25** 2069–93

Dieter C A, Maupin M A, Caldwell R R, Harris M A, Ivahnenko T I, Lovelace J K, Barber N L and Linsey K S 2018 *Estimated use of water in the United States in 2015: U.S. Geological Survey Circular 1441* p 65

Dooge J C I 2009 Fresh Surface Water, Encyclopedia of Life Support Systems. Available at:https://epa.gov/report-environment/fresh-surface-water(Accessed: 8 November 2021)

Duan K, Caldwell P V, Sun G, Mc Nulty S G, Zhang Y, Shuster E, Liu B and Bolstad P v 2019 Understanding the role of regional water connectivity in mitigating climate change impacts on surface water supply stress in the United States *J. Hydrol.* **570** 80–95

Fang Y and Jawitz J W 2019 The evolution of human population distance to water in the USA from 1790 to 2010 *Nat. Commun.* **10** 430

FAO 2017 Water for sustainable food and agriculture - a report produced for the G20 Presidency of Germany *Rome* Available at:https://fao.org/3/i7959e/i7959e.pdf

FAO 2020 *The State of Food and Agriculture* (Rome: FAO) (https://doi.org/10.4060/cb1447en)

Granzotti R V, Miranda L E, Agostinho A A and Gomes L C 2018 Downstream impacts of dams: shifts in benthic invertivorous fish assemblages *Aquat. Sci.* **80** 28
Grizzetti B, Pistocchi A, Liquete C, Udias A, Bouraoui F and van de Bund W 2017 Human pressures and ecological status of European rivers *Sci. Rep.* **7** 205
IPCC, Masson-Delmotte V *et al* 2021 Climate change 2021 *The Physical Science Basis. Contribution of Working Group I to the Sixth Assessment Report of the Intergovernmental Panel on Climate Change* (Cambridge: Cambridge University Press) Available at:https://ipcc.ch/report/ar6/wg1/
Kummu M, Guillaume J H A, de Moel H, Eisner S, Flörke M, Porkka M, Siebert S, Veldkamp T I E and Ward P J 2016 The world's road to water scarcity: shortage and stress in the 20th century and pathways towards sustainability *Sci. Rep.* **6** 38495
Lin Q 2011 Influence of dams on river ecosystem and its countermeasures *J. Water Resour. Prot.* **03** 60–6
Mancosu N, Snyder R L, Kyriakakis G and Spano D 2015 Water scarcity and future challenges for food production *Water* **7** 975–92
McKinnon K A and Deser C 2021 The Inherent uncertainty of precipitation variability, trends, and extremes due to internal variability, with implications for Western U.S. water resources *J. Clim.* **34** 9605–22
Nie W, Zaitchik B F, Rodell M, Kumar S V, Arsenault K R and Badr H S 2021 Irrigation water demand sensitivity to climate variability across the contiguous United States *Water Resour. Res.* **57** e2020WR027738
Palazzoli I 2022 Anthropogenic and climatic controls on surface water across the contiguous United States *Alma Mater Studiorum Università di Bologna.* Available at:http://amsdottorato.unibo.it/10199/
Palazzoli I, Montanari A and Ceola S 2022 Influence of urban areas on surface water loss in the contiguous United States *AGU Advances* **3** e2021AV000519
Paterson W, Rushforth R, Ruddell B, Konar M, Ahams I, Gironás J, Mijic A and Mejia A 2015 Water footprint of cities: a review and suggestions for future research *Sustainability* **7** 8461–90
Pekel J-F, Cottam A, Gorelick N and Belward A S 2016 High-resolution mapping of global surface water and its long-term changes *Nature* **540** 418–22
Pervez M S and Brown J F 2010 Mapping irrigated lands at 250-m scale by merging MODIS data and national agricultural statistics *Remote Sensing* **2** 2388–412
Poff N L, Allan J D, Bain M B, Karr J R, Prestegaard K L, Richter B D, Sparks R E and Stromberg J C 1997 The natural flow regime *Bio. Science* **47** 769–84
Rodell M, Famiglietti J S, Wiese D N, Reager J T, Beaudoing H K, Landerer F W and Lo M-H 2018 Emerging trends in global freshwater availability *Nature* **557** 651–9
Scanlon B, Rateb A, Pool D, Sanford W, Save H, Sun A, Long D and Fuchs B 2021 Effects of climate and irrigation on GRACE-based estimates of water storage changes in major US aquifers *Environmental Research Letters,* **16** 094009
Seaber P R, Kapinos F P and Knapp G L 1987 Hydrologic unit maps Water Supply paper 2294, 63
Shi X, Qin T, Nie H, Weng B and He S 2019 Changes in major global river discharges directed into the ocean *Int. J. Environ. Res. Public Health* **16** 1469
Da Silva G C X, de Abreu C H M, Ward N D, Belúcio L P, Brito D C, Cunha H F A and da Cunha A C 2020 Environmental impacts of dam reservoir filling in the East Amazon *Frontiers in Water* **2**
Singer M B, Asfaw D T, Rosolem R *et al* 2021 Hourly potential evapotranspiration at 0.1° resolution for the global land surface from 1981-present *Sci Data* **8** 224
Starr G and Levison J 2014 Identification of crop groundwater and surface water consumption using blue and green virtual water contents at a subwatershed scale *Environmental Processes* **1** 497–515
Sun G and Caldwell P 2015 Impacts of Urbanization on Stream Water Quantity and Quality in the United States *Water Resources IMPACT* **17** 17–20
Thenkabail P S, Dheeravath V, Biradar C M, Gangalakunta O R P, Noojipady P, Gurappa C and Li Y 2009 Irrigated area maps and statistics of India using remote sensing and national statistics *Remote Sensing,* **1** 50–67
Thornton M M, Shrestha R, Wei Y, Thornton P E, Kao S and Wilson B E 2020 *Daymet: annual climate summaries on a 1-km grid for North America, Version 4* (ORNL DAAC, Oak Ridge: Tennessee, USA) (https://doi.org/10.3334/ORNLDAAC/1852)
Tidwell V, Moreland B, Shaneyfelt C and Kobos P 2017 Mapping water availability, cost and projected consumptive use in the Eastern United States with comparisons to the West *Environ. Res. Lett.* **13** 014023
Vörösmarty C J *et al* 2010 Global threats to human water security and river biodiversity *Nature* **467** 555–61
Wada Y *et al* 2017 Human–water interface in hydrological modelling: current status and future directions *Hydrol. Earth Syst. Sci.* **21** 4169–93
Wang X *et al* 2020 Gainers and losers of surface and terrestrial water resources in China during 1989–2016 *Nat. Commun.* **11** 3471
Wang X and Xie H 2018 A review on applications of remote sensing and geographic information systems (gis) in water resources and flood risk management *Water* **10** 608
Yamazaki D, Trigg M A and Ikeshima D 2015 Development of a global ~90 m water body map using multi-temporal Landsat images *Remote Sens. Environ.* **171** 337–51
Zhuang X W, Li Y P, Nie S, Fan Y R and Huang G H 2018 Analyzing climate change impacts on water resources under uncertainty using an integrated simulation-optimization approach *J. Hydrol.* **556** 523–38